Effect of Polymer Architecture on the Adsorption and Coating Stability on Heterogeneous Biomimetic Surfaces

Irene Adroher-Benítez, Tatiana I Morozova, Gabriel Catalini, Nicolás A García, Jean-Louis Barrat, Gustavo S Luengo, Fabien Léonforte

Effect of polymer architecture on the adsorption and coating stability on heterogeneous biomimetic surfaces

Irene Adroher-Benítez,[†] Tatiana I. Morozova,[‡] Gabriel Catalini,[¶] Nicolás A. García,[¶] Jean-Louis Barrat,[§,‡] Gustavo S. Luengo,[*,‖] and Fabien Léonforte[*,‖]

[†]*Biocolloid and Fluid Physics Group, Department of Applied Physics, University of Granada, 18071 Granada, Spain*

[‡]*Institut Laue-Langevin, 38042 Grenoble, France*

[¶]*Instituto de Física del Sur (IFISUR), Departamento de Física, Universidad Nacional del Sur (UNS), CONICET, Av. L. N. Alem 1253, B8000CPB - Bahía Blanca, Argentina*

[§]*Laboratoire Interdisciplinaire de Physique, Université Grenoble Alpes-CNRS, 38000 Grenoble, France*

[‖]*L'Oréal Research and Innovation, Aulnay-Sous Bois, 93600 France*

Abstract

This study aims to investigate the physical properties that govern polymer adsorption and desorption on chemically structured surfaces. These surfaces are considered biomimetic of natural ones that specifically exhibit a combination of hydrophobic and hydrophilic domains, like those found on hair surfaces. Understanding these processes is especially crucial when designing and developing new eco-sustainable polymers for industrial applications such as cosmetic products. In this work, we developed computational models of the hair surface and two polymers with different architectures. The first polymer studied was a semi-flexible, linear polysaccharide of natural origin, which offers potential for sustainable formulations. The second, and more complex model, was a stiff, comb-like cationic polyelectrolyte similar to petroleum-based polymers traditionally used in hair care cosmetics. We conducted coarse-grained molecular dynamics simulations to study the adsorption of the polymers onto the substrate and we found that increasing polymer concentration enhanced adsorption. The branched copolymer led to a thicker coating and exhibited a more random coverage pattern compared to the linear polymer. Furthermore, we analyzed the stability of the polymer coating by running Brownian dynamics simulations of the adsorbed polymers under a linear shear flow. These simulations revealed a correlation between flow strength and polymer desorption, thereby highlighting the importance of low desorption time for performing coatings in cosmetic applications. Despite both polymer types presenting improved resistance with longer polymer chains, the branched polymer layer exhibited higher stability. This finding demonstrates the key role of polymer architecture in assessing the coating formation, properties and performance of new eco-sustainable polymers in industrial applications.

Introduction

Research in eco-friendly cosmetic formulations is a growing field due to an increasing consumer demand for innovative products that establish a compromise between efficiency and sustainability. It is critical to align this research with the principles of green chemistry,[1] emphasizing the design and production of safe, biodegradable, and efficient polymers, and minimizing the use of harmful compounds. Certain ingredients currently used in cosmetic products, like silicones and cationic polyelectrolytes, such as polyquaterniums,[2] present considerable ecological challenges.[3] These difficulties have driven the cosmetic industry to improve sustainability in their formulations. However, transitioning from existing polymers to greener alternatives is non-trivial, as the new components must meet the performance standards expected by consumers. Still, progress has been made in this direction, since some polysaccharides have already been incorporated into makeup formulations.[4] Indeed, carbohydrates represent promising sources of sustainable monomers. Despite the economic challenges they pose when competing with petrochemical-derived polymers, there are many opportunities to improve their value in high-demand applications through targeted property enhancements.[5] Recognizing these opportunities, the cosmetic industry has been actively conducting research on the synthesis and application of such green polymers.[6] Certainly, an interdisciplinary collaboration between fundamental and applied research is crucial for achieving this objective.

A part of this effort must be dedicated to identifying the physical parameters that govern polymer adsorption onto hair-like substrates. The first challenge is therefore to have a good knowledge of the hair surface, which is made of many layers.[7] The most external layer, that acts as physical and chemical protection for the hair, is called the F-layer.[8] It is formed by fatty acids and it is hydrophobic.[9] This layer can be partially damaged by several factors, including ageing and external aggressions such as solar radiation, bleaching, and various treatments.[10–13] The cuticle degradation exposes hydrophilic layers of hair, resulting in a surface that exhibits both hydrophobic and hydrophilic areas.[14,15] Surface heterogeneity can significantly influence the dynamics of molecule adsorption, thereby affecting the physical properties of the resulting coatings.[16,17] In the context of cosmetics, the diverse physicochemical characteristics across different regions of the hair surface make uniform polymer adsorption a considerable challenge. Addressing this substrate complexity, Llamas et al.[18] conducted experimental research on the adsorption of polymer and surfactant mixtures for personal care products, focusing on the interaction with different hair surfaces. They introduced systems capable of adhering to negatively charged surfaces, paving the way for new methods of applying cosmetic ingredients.

The equilibrium properties of polymer coatings and the dynamics of polymer adsorption have sustained interest from the scientific community for years. Pioneering experimental work, such as the study conducted by Frantz and Granick on the adsorption-desorption kinetics of polymers at a solid surface,[19] has provided insight into the factors that influence the dynamics of adsorbed polymer chains. However, theoretical and computational methods can offer some advantages over experimental research, including reduced cost and time, or improved precision and scalability. For instance, Polotsky and Ivanova conducted a series of analytical studies on the adsorption of single polymer chains onto stripe-patterned surfaces to investigate the adsorption-desorption transition. They developed different theoretical models for homopolymers[20,21] and copolymers,[22] and analyzed the effect of parameters such as temperature, chain stiffness or polymer composition on the adsorption on these heterogeneous surfaces. Milchev and Binder[23] conducted molecular dynamics simulations to clarify how chain stiffness influences the adsorption transition and structural properties of adsorbed semiflexible polymer chains. With a focus in cosmetic

applications, Banerjee et al.[24] investigated the deposition of cationic polyelectrolytes from micellar solutions containing surfactants onto hair-like surfaces. Using self-consistent field calculations, they found that polyelectrolyte adsorption is typically governed by the molecular details of the species in solution as well as the specificities of the surface. They highlighted the critical role of molecular modeling in optimizing the adsorption processes in industrial applications. Molecular dynamics was also used by Zhou et al.[25] to investigate how the strength of substrate attraction and polymer chain length affected the behavior of adsorbed and non-adsorbed chains in substrate-supported thin films. They found an influence zone beyond which the diffusion of polymer chains remained unaffected by the substrate. The adsorbed polymer layer comprised a fraction of weakly adsorbed chains with tails that extended vertically, penetrating the non-adsorbed chains. Interestingly, the ends of these chains were found to have a notable impact on the dynamics of the free polymers in the bulk.

Studying the rheological effects of polymer adsorption and desorption in flowing systems represents a relevant area of interest, especially within the context of hair and skin cleaning products. These cosmetics are typically applied under the influence of a shear flow. In general, it is expected that the flow enhances the desorption of the adsorbed polymer layers, while hydrodynamic forces could potentially inhibit the adsorption of polymer chains onto surfaces from flowing solutions.[26] Recent computational studies have made progress in understanding polymer adsorption and desorption in flowing systems. Panwar and Kumar[27] utilized coarse-grained Brownian dynamics simulations to analyze the adsorption of a polyelectrolyte onto an oppositely charged surface. They examined adsorption behavior with respect to screening length in presence and absence of shear flow. Under shear flow, they observed the polymer chain aligning with the flow direction, increasing surface contact. An investigation by Ibáñez-García et al.[28] focused on how attractive surfaces affect the stretching of confined tethered polymers under shear flow. They observed unique stationary cyclic dynamics, varying with the shear flow intensity and surface potential strength. Their results indicated that a stronger attractive potential decreased polymer stretching, deviating from scaling predictions for non-adsorbed polymers. They also found the shear flow intensity to enhance the adsorption process. Šindelka et al.[29] employed dissipative particle dynamics simulations for study of the interaction between two main components of personal care products and the human hair surface. Their work included analysis both above and below the fluid-gel transition temperature and both in- and out-of-equilibrium conditions. Interestingly, under shear stress, they found that beyond a certain threshold, both types of adsorbed layers began to lose their attached molecules. In the fluid layers, this was due to increased shear overpowering the hydrophobic interactions, while in the gel layers, it resulted from the collapse of the hair lipid brush, causing a significant desorption.

Understanding the friction between hair fibers and polymer-coated hair surfaces is also of significant scientific and industrial importance. The degree of friction influences the tactile sensation, manageability, and combing of hair, which are primary factors in consumer perception of hair care products. Recently, Weiand et al.[30] investigated the nanoscale friction between biomimetic hair surfaces using experiments and coarse-grained molecular dynamics simulations. In the simulations, friction was monitored between hair surfaces with different levels of chemical damage. They found that the increase in nanoscale friction in chemically damaged hair is primarily due to changes in the hair surface chemistry, not because of changes in either its roughness or damage beneath the surface. On the other hand, Coscia et al.[31] investigated the tribological behavior of diffferent polymers in surfactant solutions in contact with the hair surface, comparing the aggregation behaviour and lubrication properties of a generic functionalized polysaccharide with two petroleum-based polyelectrolytes used in shampoo formulations.

In our previous work, we examined the adsorption of hydrophilic flexible homopolymers to surfaces that chemically mimic human hair.[32] By merging experimental imaging data with coarse-grained molecular dynamics simulations, we explored the impact of polymer chain length and concentration on the adsorption process. We observed that an increase in concentration led to longer polymer tails and loops, reducing the length of the chain sections attached to the surface. We also tested the stability of these polymers under a linear shear flow. Advancing from this foundation, our current study serves as a natural extension, introducing more complex and realistic polymer models to verify the robustness of the computational framework. Our research includes the effect of different polymer architectures, concentrations, and chain length on polymer adsorption. Simulations of rinsing under a linear shear flow were also performed. By considering various flow strengths, we systematically probed the desorption dynamics. This investigation represents a significant step in the construction of models for complex macromolecules interacting with realistic biological surfaces, with the ultimate goal of promoting the design of more eco-friendly industrial products.

The structure of this manuscript is as follows. After this introduction, we detail the models and methodologies employed in our study. This includes descriptions of the substrate and polymer models we have developed, as well as the simulation techniques implemented to model polymer adsorption. The subsequent section presents our findings in the context of the various variables explored, namely polymer architecture, monomer concentration, chain length, and flow strength. We provide interpretations and discuss these results. Finally, we draw conclusions and propose possible directions for future research.

Model and methods

Substrate model

The essential simulation setup consisted of a polymer solution with a substrate at the bottom of the simulation box. Based in real dynamic Chemical Force Microscopy images, the substrate was modeled to represent a realistic bleached human hair surface.[14] Therefore, 60% was composed of damaged areas, which were hydrophilic, while 40% was composed of healthy hydrophobic zones. Figure 1 shows the substrate model used in this work. It was made of spherical beads with the same size as polymer beads, labeled as G (hydrophilic) and H (hydrophobic). For more detailed information regarding the construction of this model, we refer the interested reader to to the previously published paper by Morozova et al.[32]

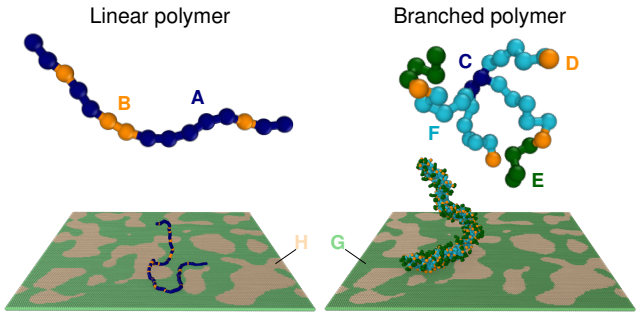

Figure 1: Computational models for the (left) linear and (right) branched polymers. Snapshots on top show (left) a section of the linear polymer with 15 beads, each one representing one monomer, and (right) a dimer of the branched polymer with 17 beads per monomer. Bottom pictures show a single polymer composed by N=150 monomers adsorbed onto the heterogeneous substrate.

Polymer models

We developed two polymer models that correspond to a semi-flexible linear polymer of natural origin and a stiff branched polymer with a bottle-brush structure, similar to those currently used in cosmetic formulations. The former was modeled after chitosan, a linear polysaccharide composed of randomly distributed deacetylated and acetylated units. For the latter, we took inspiration from polyquaterniums, a family of polycationic polymers with quaternary ammonium centers.

Linear block copolymer

We modeled a semi-flexible linear block copolymer where each bead represents a monomer: either D-glucosamine (GlcN) or N-acetylglucosamine (GlcNac) proving the notion of the length-scale in simulations as the size of the monomer is approximately 0.5 nm.[33] In this model, GlcN units are described by positively charged A beads, while hydrophobic electroneutral B beads stand for GlcNac monomers[34](see Figure 1). In experiments, polymers like chitosan are composed of 80% GlcN. In our model we have preserved this same fraction of A beads, which are randomly distributed along the chain. We considered good solvent conditions for the chains, resulting in a purely repulsive Weeks-Chandler Andersen (WCA)-type interaction among all monomers

$$U_{\mathrm{WCA}}(r_{ij}) = 4\varepsilon\left[\left(\frac{\sigma}{r_{ij}}\right)^{12} - \left(\frac{\sigma}{r_{ij}}\right)^{6}\right] + \varepsilon, \quad r_{ij} < r_c = 2^{1/6}\sigma, \tag{1}$$

where ε is the interaction strength, and r_{ij} is the distance between i and j monomers. For distances $r_{ij} \geq r_c$, $U_{\mathrm{WCA}}(r_{ij}) = 0$. In addition, neighboring monomers were connected via the finitely extensible nonlinear elastic (FENE) potential

$$U_{\mathrm{FENE}}(r_{ij}) = -\frac{1}{2}\kappa r_0^2 \ln\left[1 - \left(\frac{r_{ij}}{r_0}\right)^2\right], \tag{2}$$

where we employed the standard Kremer-Grest parameters to prevent unphysical bond crossing, i.e. the maximum bond extension is set to $r_0 = 1.5\sigma$, and $\kappa = 30\varepsilon/\sigma^2$ is the spring constant.[35] Chitosan is a semiflexible polymer with persistence length of approximately $l_{\mathrm{p}} \simeq 9$ nm for the chain composition investigated.[36] Thus, we introduced a bending potential of the harmonic form

$$U(\theta)_{\mathrm{bend}} = \frac{1}{2}k(\theta - \theta_0)^2, \tag{3}$$

where $\theta_0 = 2\pi$, and the potential constant $k = 18\ \varepsilon/rad^2$. The value of k was chosen in a such a way, that the resulting l_{p} of a chain in simulations is close to the experimental value, i.e., $l_{\mathrm{p}}^{\mathrm{sim}} = 18\sigma$.

Furthermore, under experimental conditions, i.e., pH 4.5, chitosan is positively charged through the protonation of its GlcN monomers.[34] Hence, we assumed that each A bead carries a positive elementary charge, $z_A = +1$. We used the experimentally determined value of the surface charge of a hydrophilic zone of bleached hair[11] to estimate the charge of hydrophilic G beads. According to our calculations, each G bead has $z_G = -0.11$ elementary charge. Since under experimental conditions the aqueous solution contains salt ions, we described the effective interaction between two charged beads through the Debye-Hückel screened electrostatic potential,

$$U_{\mathrm{DH}} = \frac{z_A z_G l_{\mathrm{B}}}{r} e^{-\kappa r}, \tag{4}$$

where $l_{\mathrm{B}} = \dfrac{e^2}{4\pi\varepsilon\varepsilon_0 k_{\mathrm{B}} T}$ is the Bjerrum length, and κ is the inverse Debye length. We adopted experimental values of $l_{\mathrm{B}} = 0.7$ nm, and $1/\kappa = 1.0$ nm.

Lastly, the excluded-volume interactions between charged A beads and two types of the substrate beads, as well as between hydrophobic B beads and G (hydrophilic) substrate beads, are given by WCA poten-

tial introduced above. Interaction between hydrophobic monomers and hydrophobic beads of the substrate includes attractive part and is described by the Lennard-Jones (LJ) potential

$$U_{\mathrm{LJ}}(r_{ij}) = 4\varepsilon_{\mathrm{ms}}\left[\left(\frac{\sigma}{r_{ij}}\right)^{12} - \left(\frac{\sigma}{r_{ij}}\right)^{6}\right], \quad r_{ij} < 3\sigma, \tag{5}$$

where the value of the energy well was taken from our former study of the homopolymer adsorption and results in $\varepsilon_{\mathrm{ms}} = 0.3\varepsilon$.[32]

Branched bottle-brush copolymer

We also modeled a cationic polyelectrolyte like those currently used in hair cosmetics. It has a stiff comb-like architecture in which each monomer is made of 17 beads. Figure 1 (right) shows a dimer of this polymer. The backbone of the chain is made of amphiphilic C beads, while the branches contain charged hydrophilic D beads, hydrophobic E and electroneutral F beads. As for the other polymer model, we considered good solvent conditions, that results in a purely repulsive interactions among all monomers modeled via WCA potential. Neighboring monomers are connected via FENE potential. Amphiphilic C beads of the monomer interact via LJ potential with all substrate beads with the strength $\varepsilon_{\mathrm{ms}} = 0.3\varepsilon$. Charged D beads interact only with charged beads of the substrate (G) using Debye-Hückel potential, where the charge for D beads $z_D = 1.4$ is adopted. All other interactions between monomeric and substrate beads are described by the excluded-volume interactions (WCA potential). In Table 1 we summarize all monomer types employed in this study.

Table 1: Description of monomer beads employed including their physical nature and type of attractive interaction with the substrate.

Name	Polymer	Physical nature	Interactions
A	Linear	Charged	U_{DH}
B		Hydrophobic	U_{LJ}
C	Branched	Amphiphilic	U_{LJ}
D		Charged	U_{DH}
E		Hydrophobic	U_{LJ}
F		Neutral	U_{WCA}

Simulations

With these two polymer families and the modeled substrate we performed coarse-grained molecular dynamics simulations with implicit solvent. The simulation box had periodic boundary conditions in x and y directions and was confined in z direction, normal to the surface. All the simulations were performed within the canonical NVT ensemble. To model the dynamics of the polymers in bulk and adsorbing onto the substrate we used a Langevin thermostat, while the effect of a linear shear flow on the adsorbed polymer chains was simulated applying Brownian dynamics. Simulations were run by means of the simulation package HOOMD-blue.[37]

Table 2 summarizes the sets of system parameters explored in the simulations, namely: polymer architecture, concentration and length to study the adsorption onto the substrate, as well as flow strength to test the stability of the adsorbed layer. First, as described above, we chose two distinct polymer types with different architectures: a semi-flexible linear block copolymer, henceforth referred to as the linear polymer, and a stiff comb-like cationic polyelectrolyte, which we shall designate as the branched polymer. We studied three monomer concentrations ranging from dilute solutions to semidilute ones, $c/c^* = \{0.1, 0.5, 1.0\}$, being c^* the overlap concentration,

$$c^* = \frac{N}{\frac{4}{3}\pi R_{\mathrm{g0}}^3}, \tag{6}$$

where N is the number of monomers per chain and R_{g0} is the polymer gyration radius at infinite dilution. To assess the effect of the degree of polymerization on the dynamics of polymer adsorption and on the stability of the polymer coating, we considered three different polymer lengths, characterized by the number of monomers per chain, $N = \{150, 250, 500\}$. To have statistically significant results, for each system configuration we ran three independent simulations.

Table 2: Polymer architecture, concentration and length, as well as Weissenberg numbers explored in the simulations performed in this study.

Simulation	Polymer	c/c^*	N	Wi
Adsorption	Linear Branched	0.1	150	
		0.5	250	
		1.0	500	
Desorption	Linear Branched	1.0	150	0.5
				1.0
			250	5
			500	10

The stability of the resulting polymer coating was analyzed applying a linear shear flow along the x-axis to the adsorbed polymers chains. Theoretical and computational details of these calculations can be found in our former work.[32] To examine the desorption of polymer chains under applied shear flow, we selected a sample from all the adsorption simulations we conducted, as summarized in Table 2. The concentration was set to $c/c^* = 1.0$, based on the assumption that the density within the adsorbed polymer layer is uniform, a requirement for solving the Brinkman equation.[38,39] The polymerization degrees studied during the desorption simulations were the same as those used in the adsorption simulations, namely $N = \{150, 250, 500\}$ monomers per chain. To characterize the strength of the flow we used the Weissenberg number $Wi = \dot{\gamma}\tau_0$, where $\dot{\gamma}$ is the ap-

plied shear rate and τ_0 is the chain relaxation time at infinite dilution.[40] Further details regarding the computation of τ_0 are provided in the Supplementary Information. Since the Weissenberg number provides the degree of anisotropy generated by the flow, we assume that $Wi > 1$ implies a strong shear flow, while $Wi \leq 1$ indicates a weak perturbation.

The complete workflow of this study is summarized in Figure 2. First, the adsorption of the polymer solution onto the heterogeneous substrate was simulated. Non-adsorbed polymers were then removed to obtain the resulting coating. Subsequently, a linear shear flow was applied to the adsorbed layer. Figure 2(c) shows the desorbed polymers colored in pink. The final state of the coating with the remaining adsorbed polymers is presented in Figure 2(d). It is worth noting that during the simulation of a linear shear flow applied to the system, the longest polymer chains were stretched under strong flow regimes which led to polymer self-interaction within the simulation box. To address this issue, the simulation box was duplicated in the flow direction.

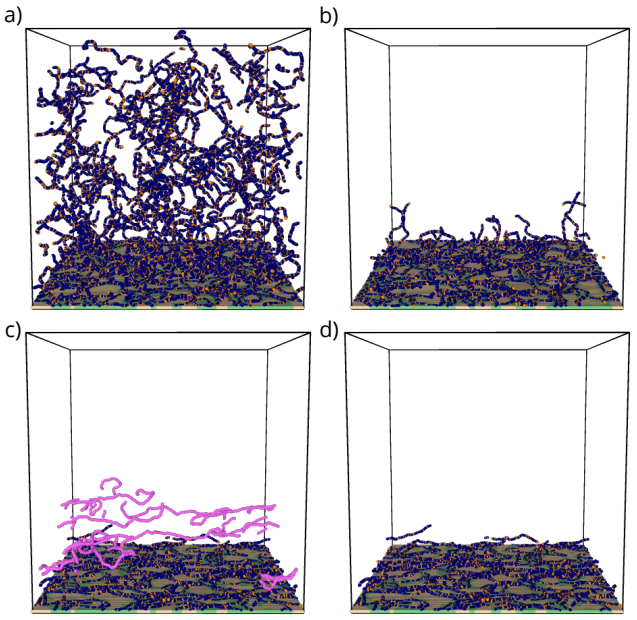

Figure 2: Snapshots of different stages of the simulations for linear polymers of length $N = 250$ at concentration $c/c^* = 1.0$. (a) Adsorption of the polymer solution on the substrate. (b) Resulting adsorbed polymer layer. (c) Simulation of the applied shear flow on the adsorbed layer, where desorbed polymers have been colored in pink. (d) Final state of the coating with the remaining adsorbed polymers.

Results and discussion

To ensure that the results obtained from the simulation of two distinct polymer types with different architectures were comparable, we first conducted simulations of polymers in solution for all the system configurations explored in this study. We measured the radius of gyration in bulk, as shown in Figure 3, and confirmed that the sizes of the polymers were similar for a given degree of polymerization N. The obtained results allow us to confidently compare the behavior of these two polymer types and gain insights into the properties of the adsorbed layers. Additionally, by fitting the data to a linear function we determined the value of the radius of gyration of the polymer at infinite dilution R_{g0} from the y-intercept, used in the calculation of the overlap concentration in equation (6).

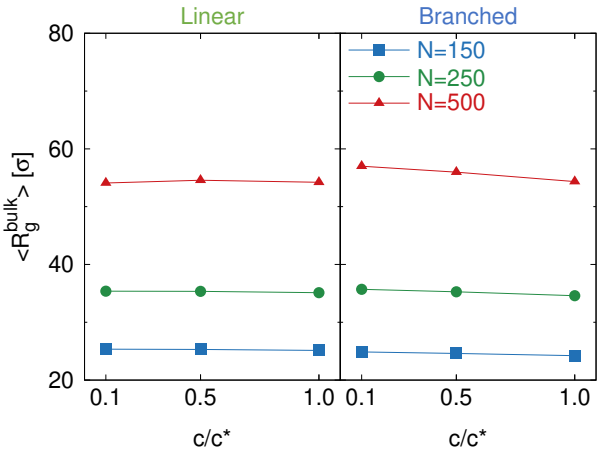

Figure 3: Radius of gyration of both polymer types as a function of concentration for different chain lengths. Left plot represents the linear polymer, while the right plot represents the branched polymer. The red triangles, green circles, and blue squares in each plot correspond to the data for the chains with degree of polymerization $N = 500$, $N = 250$, and $N = 150$, respectively.

After confirming that both types of polymers were of comparable size, we proceeded to examine their adsorption strength with the substrate. To do so, we calculated the mean potential energy u_{ads} between a monomer from an adsorbed chain and the substrate. This calculation was performed on the polymer coatings obtained at the end of the adsorption simulations, after all non-adsorbed chains had been removed from the simulation box. The results revealed that the adsorption strength per monomer for both polymer models was nearly identical: $u_{\text{ads}} = (0.46 \pm 0.02)\varepsilon$ for the linear polymers and $u_{\text{ads}} = (0.44 \pm 0.01)\varepsilon$ for the branched polymers. The similarity in adsorption strength suggests that any observed differences in the properties of the coatings formed by these polymers could be attributed to other factors, such as differences in polymer architecture.

As the first step in the characterization of the polymer coatings, we started by computing the concentration profiles of the adsorbed chains as a function of the distance to the substrate. These profiles are plotted in Figure 4(a) at three different concentrations for three types of polymers with $N = 500$ monomers per chain: the linear and branched copolymers modeled in this study, and the linear flexible homopolymers analyzed in our previous study.[32] To enable comparison of the

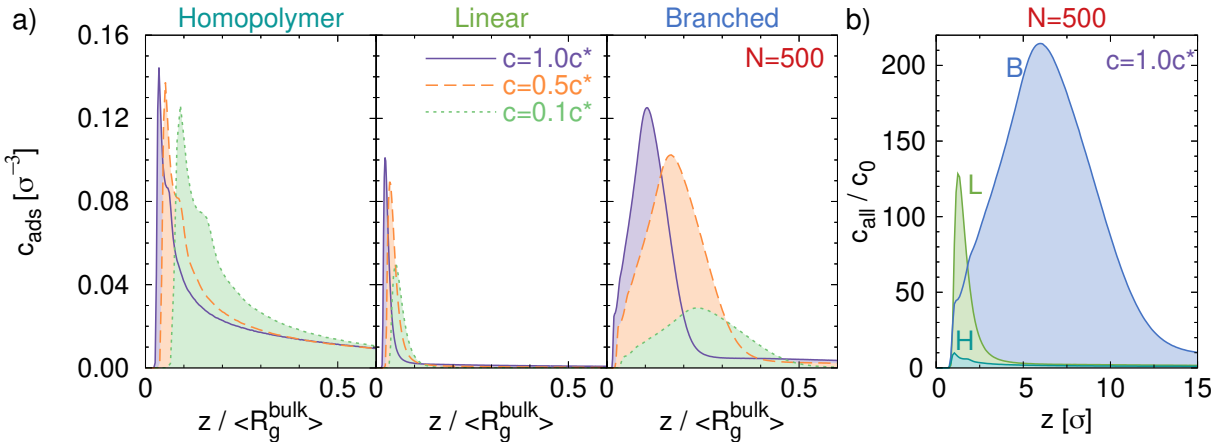

Figure 4: Concentration profiles of polymers as a function of the distance from the substrate. (a) Profiles of only the adsorbed polymers for three polymer types with a chain length of $N = 500$ at three different concentrations. (b) Concentration profile of the three different polymer solutions normalized by the bulk concentration at $c/c^* = 1.0$.

resulting layers, the distance in the figure is normalized by the mean radius of gyration of chains in solution. We found that the shape of the profiles remained constant with concentration for all polymer types, while polymer adsorption increased with concentration. Nevertheless, we could expect the concentration to reach a threshold value that saturates the substrate, preventing more polymers to adsorb. When comparing the polymer types, it was observed that the semi-flexible linear copolymer generated a significantly less thick coating with respect to the average chain length compared to the flexible homopolymer and the branched copolymer. This is because both the linear homopolymer and the branched copolymer, when adsorbed on the substrate, still had long tails that were not adsorbed, contributing to the concentration profile far from the substrate. Conversely, for the linear copolymer, the portion of chain adsorbed onto the substrate was larger, leading to shorter tails in comparison to the average size of the polymers in solution. These findings demonstrate the importance of considering not only polymer architecture but also the specific monomer-substrate interaction in understanding the adsorption dynamics and properties of polymer coatings. Figure 4(b) contains the concentration profiles normalized by the bulk concentration of the three polymer solutions at $c/c^* = 1.0$ as a function of the absolute distance to the substrate. The rapid rise in the concentration profiles at small distances confirms that, in all cases, chains exhibit a preference for adsorption onto the substrate rather than dispersion in the bulk. Furthermore, the concentration profiles also indicate that the branched copolymer is notably more voluminous than the linear polymers, which contributes to the formation of a thicker polymer layer.

To determine the uniformity of the polymer coverage on the substrate, we performed a novel analysis method. The simulation box was partitioned into several slabs along z-axis and the monomer density profile was calculated in each point in the slab. These profiles were then integrated over the slab thickness to obtain two-dimensional density profiles, which were averaged over multiple snapshots of the simulation trajectory. Further details, including an explanatory figure of this slab analysis method, can be found in the Supporting Information. Figure 5 shows the results obtained by dividing each adsorbed polymer layer into four slabs of equal thickness. The first slab starts at a distance zero from the substrate and the last slab ends at a distance h_{ads}, which is the average thickness of the adsorbed polymer layer. It is observed that as the chain length increases, the polymer coating becomes denser and it is easier to keep track of the chains at further slabs from the surface due to reduced mobility and longer tails. For branched polymers the effect of chain length is more significant due to their bulkier nature. Analysis of the slabs close to the substrate shows that for short chains the branched polymers can accommodate in the substrate, while for chains with $N > 150$ mobility seems to be significantly restricted due to overcrowded substrate. The figure also reveals that linear polymers exhibit a higher degree of memory of the substrate compared to the branched ones. The linear chains adhere more strongly to the hydrophilic areas of the substrate and clearly follow its heterogeneous pattern, resulting in a clear correlation between the polymer layer and the substrate. This effect is particularly evident for long chains. Conversely, branched polymers show a more homogeneous distribution on the substrate. This effect can be attributed to the difference in the chain architecture between linear and branched copolymers, as well as to the specific monomer-substrate interactions. The linear chains have a semi-flexible structure and are made mostly of positively charged monomers, so they are strongly attracted by the hydrophilic beads of the substrate and can also easily adapt to the pattern. Instead, the stiff and voluminous structure of branched polymers limits their mobility and the intricate architecture of each monomer leads to a more complex overall monomer-substrate interaction.

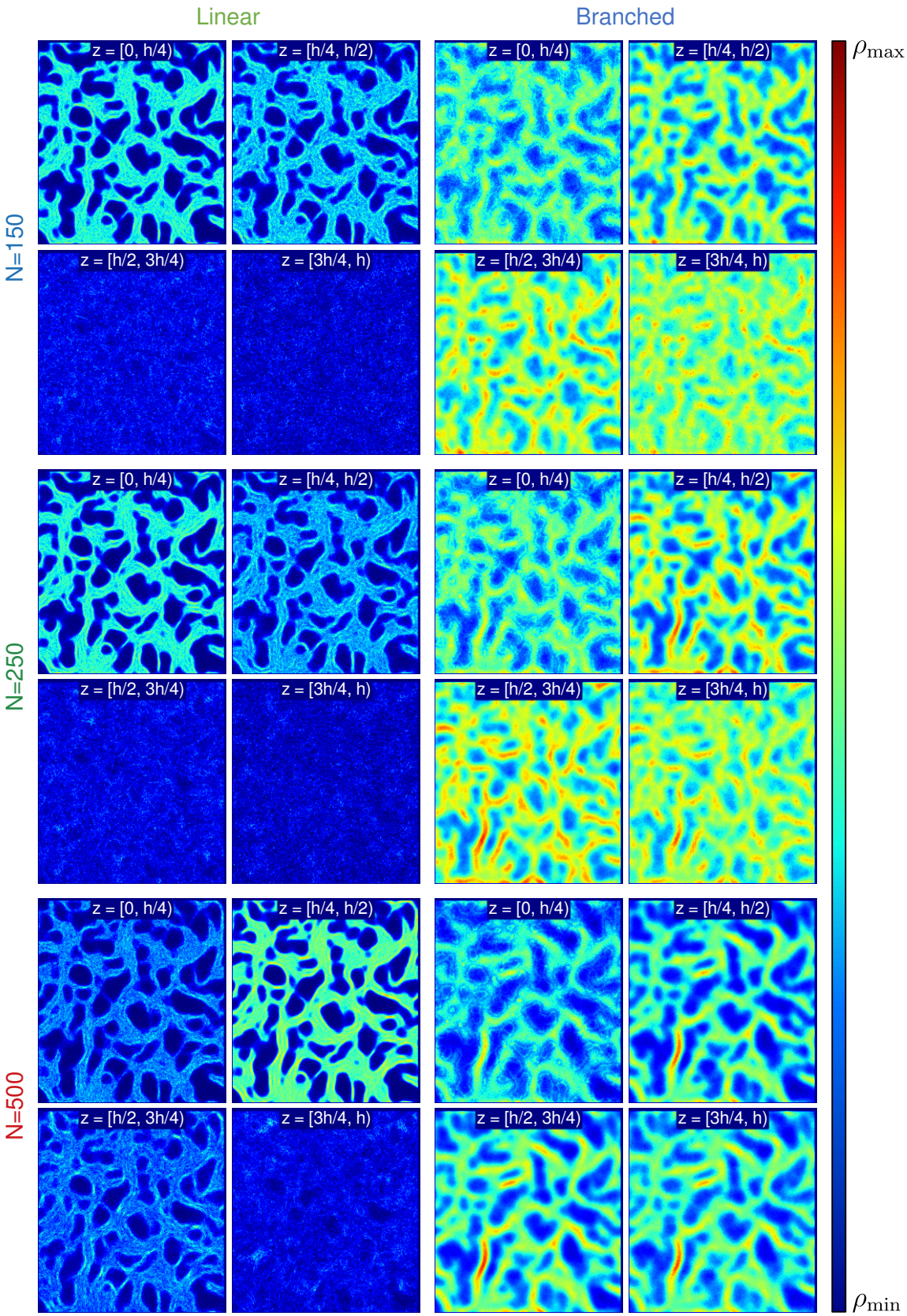

Figure 5: 2D monomer density profiles obtained by dividing the polymer coating in four slabs of height one fourth of the average thickness of the adsorbed polymer layer (h_{ads}). For each system configuration, the first slab starts at a distance zero from the substrate and the last slab ends at a distance h_{ads}. The color scale represents the total monomer density, with warmer colors indicating higher density. Note that the color scale limits vary across panels, with the maximum and minimum values adjusted to best show the range of density in each panel. In this figure we have selected one system for each polymer family and chain length at concentration $c/c^* = 0.5$.

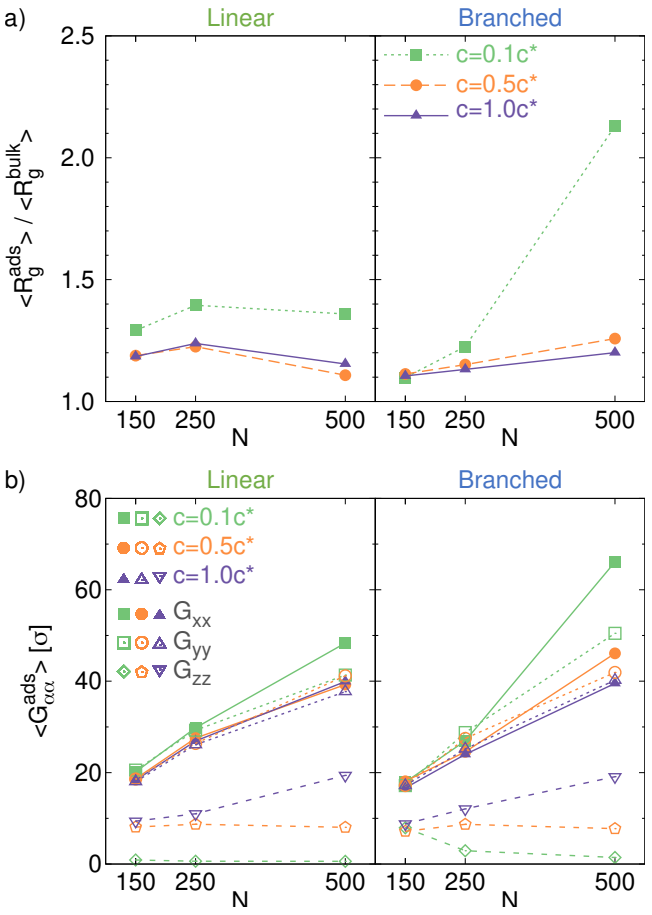

Figure 6: (a) Mean radius of gyration of the adsorbed polymers normalized by their values in bulk as a function of chain length. (b) Diagonal components of the gyration tensor as a function of chain length (N) for three different concentrations. Green symbols correspond to $c = 0.1c^*$, orange symbols to $c = 0.5c^*$ and violet symbols to $c = 1.0c^*$. Filled squares, circles and triangles represent G_{xx} at the three mentioned concentrations, while empty squares, circles and triangles represent G_{yy}. The values for G_{zz} are indicated with empty diamonds, pentagons and inverted triangles.

Figure 6(a) displays the mean radius of gyration of the adsorbed polymers normalized by the bulk values as a function of chain length N for three different concentrations. We found that the radius of gyration is larger for polymers when they are adsorbed on the substrate than when they are free in bulk, in all cases. This increase in size can be attributed to the change of the chain geometry when adsorbed. We also observed that the degree of polymerization of the chains does not make a significant difference in any case, except for very long branched polymers at very low concentrations. To further understand the change in the geometry of the polymers when adsorbing, we examine Figure 6(b), which shows the diagonal components of the gyration tensor. These quantities provide information about the dimension of the polymer along the Cartesian axes. The component G_{zz} is normal to the substrate and, since we are considering only adsorbed chains, it is expected to have a low value in most cases. Indeed, as seen in Figure 6(b), the G_{zz} components are typically the smallest. With increasing concentration, we have already mentioned that the adsorption of polymers was enhanced. Therefore, the G_{zz} component increases due to chains having to compete for the available space on the substrate, thus leading to larger tails and chain loops in the z direction. On the other hand, the gyration tensor components G_{xx} and G_{yy} that are parallel to the substrate show a decrease with increasing concentration. Since for large concentrations chains were crowded together on the substrate, their geometry became more rounded and there were no preferred orientations. However, the case of the longest branched polymers at the lowest concentration is noteworthy, as the G_{xx} component is very large. This occurred because only a small number of polymers were adsorbed, which allowed the chains to fully adsorb onto the substrate. Additionally, it is important to note that since the sample size was smaller in these cases, it is possible that the stretching of the chains was overestimated.

In the following, we analyze the effect of applying a linear shear flow on the adsorbed polymer layer. Figure 7 contains the final values of the diagonal components of the gyration tensor after running the rinsing simulations. The data is normalized by the G_{xx}, G_{yy} and G_{zz} values computed for the adsorbed polymer coating before applying the shear flow, already shown in Figure 6(b). In this way the first thing we can observe is that the component G_{zz} normal to the substrate always decreases with respect to its initial value when the flow is applied, while the parallel and vorticity components (G_{xx} and G_{yy}) experience very different changes. G_{xx} is the component in the direction of the flow and it always have a higher value after the rinsing than before. On the other hand, for the component in the vorticity direction we always observe $G_{yy}/G^0_{yy} \sim 1$. This general trend can be attributed to the effect of the flow applied in the x-direction. It causes the adsorbed structures, such as chain tails and loops, to tilt towards the surface, thereby altering their overall geometry. Consequently, the diagonal component of the gyration tensor in the flow direction increases while the component in the normal direction decreases. In addition, depending on how stretched where the chains originally, the component in the vorticity direction may slightly increase or decrease. When analyzing the effect of flow strength, we observe significant differences between weak and strong shear flow regimes, particularly for branched polymers. In all cases an increase in flow strength resulted in more pronounced changes on the geometry of the adsorbed polymers. However, within the same regime, the variation in Weissenberg numbers does not appear to have a significant impact on the trend of the values in the plot. Figure 7 also reveals that the way the flow affects the adsorbed coating highly depends on the polymer architecture. Linear polymers were found to be responsive to the flow in all scenarios, even under weak flow conditions. The flow stretched the chains and tilted them towards the substrate, leading to a nearly flat coating with no polymer tails normal to the substrate in the strong

flow regime. In this case, the chains were accommodated on the substrate aligned with the flow direction, which explains the high increase of G_{xx} for the longest chains. On the other hand, the branched polymers were practically unaffected by the flow in the weak regime, which can be attributed to the denser and bulkier adsorbed layer they had created compared to the linear polymers. Indeed, the degree of polymerization plays an important role in the behavior of these polymers under strong flow regime. In Figure 7(d) we can observe that as chain length N increases the diagonal components of the gyration tensor approach their original values, that is, the initial polymer coating is less affected by the applied shear flow for longer chains. Nevertheless, below we will discuss the effect that simulation time may have if we had run the simulations for longer times.

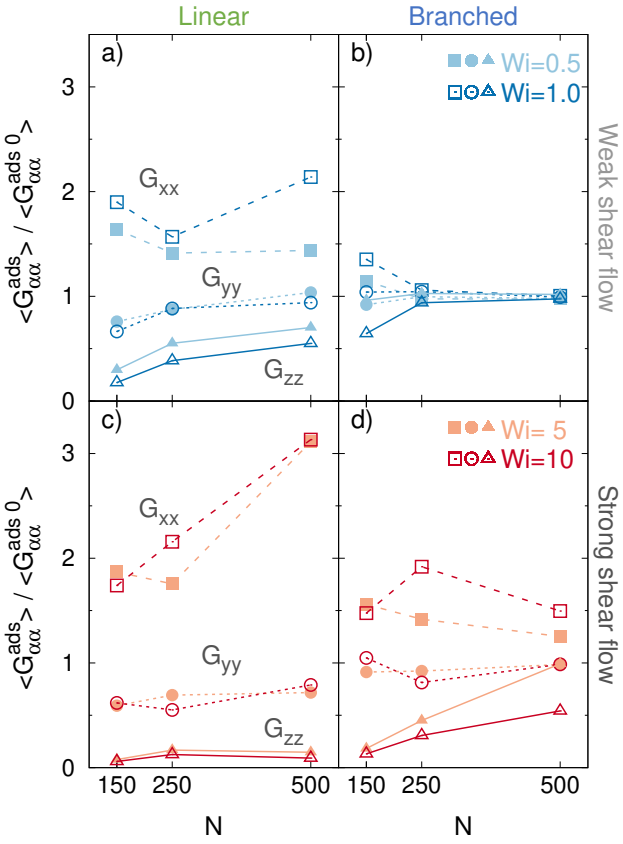

Figure 7: Diagonal components of the gyration tensor after applying a shear flow to the adsorbed polymers normalized by the initial value as a function of chain length. Left plots (a,c) show results for linear copolymers and right plots (b,d) for branched ones. Results under weak shear flow regime are shown colored in blue in top pannels (a,b), while strong flow is represented by red symbols in bottom panels (c,d). For each regime, two different Weissenberg numbers have been considered. Within each color, the light shade corresponds to the smallest Weissenberg number, while the intense shade corresponds to the highest Wi. The symbol scheme for each panel is as follows: squares represent G_{xx}, circles represent G_{yy}, and triangles represent G_{zz}.

The analysis of the time evolution of the fraction of adsorbed polymers can provide important insights into

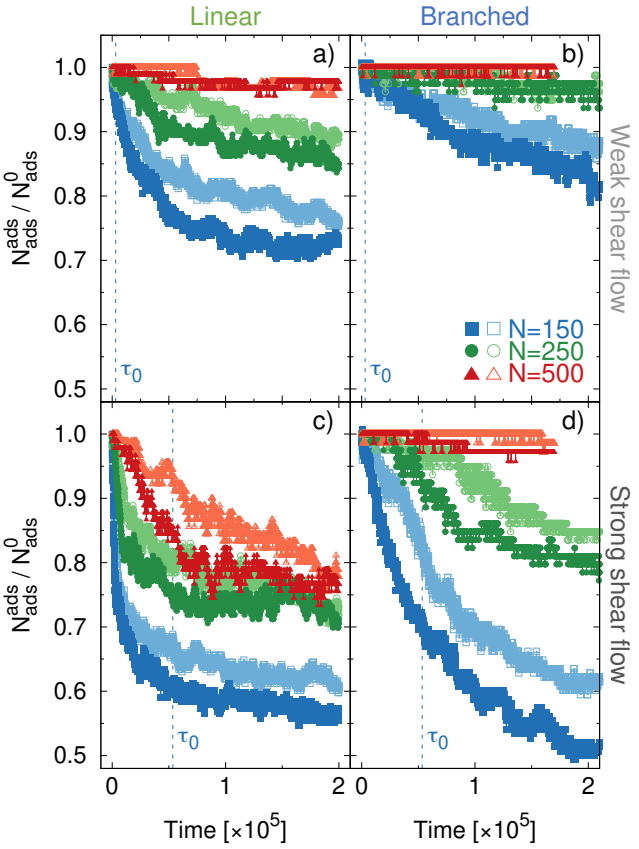

Figure 8: Fraction of adsorbed polymers on the heterogeneous substrate as a function of time. Left plots (a,c) show results for linear copolymers and right plots (b,d) for branched ones. Evolution under weak shear flow regime is shown in top pannels (a,b), while strong flow corresponds to bottom panels (c,d). For each regime, two different flows have been applied, characterized by the Weissenberg number. The color scheme for each panel is as follows: blue squares represent $N = 150$, green circles represent $N = 250$, and red triangles represents $N = 500$. Within each color, the light shade corresponds to the smallest Weissenberg number, while the intense shade corresponds to the highest Wi. As a guide, the relaxation time at infinite dilution τ_0 of chains of length $N = 150$ is indicated by a vertical dashed line.

the dynamics of polymer coatings under shear flow. Figure 8 shows the ratio between the number of adsorbed chains at a given time and the initial value of polymers adsorbed on the substrate for all the system configurations considered in this study, listed in Table 2: linear and branched copolymers of three different chain lengths and under weak ($Wi = \{0.5, 1.0\}$) and strong ($Wi = \{5, 10\}$) flow regimes. The evolution of the system was found to be more time demanding under weak flow conditions and for longer polymer chains. In particular, the branched polymer was observed to evolve at a much slower rate compared to the linear polymers, requiring a longer time to reach a steady state due to its more complex architecture. As a consequence, it was impossible to carry out the simulations of the branched polymers under shear flow for the same amount of time with respect to the polymer relaxation time at infinite

dilution τ_0 than for the linear polymers. However, this is not necessarily a drawback, since our aim is to compare the behavior of two different types of polymers with cosmetic applications in mind. To ensure a fair comparison, we report the absolute simulation times in Figure 8. Additionally, we include the value of the chain relaxation time at infinite dilution τ_0 for the smallest polymers to provide context for the overall simulation time. From the plots, we can see that some chains desorbed from the substrate in all cases studied, with a stronger flow leading to more detachment. The linear polymers desorbed much faster than the branched polymers, and stronger flows resulted in even faster desorption. Both linear and branched polymers resulted in more stable coatings when longer chains were used. Lastly, the branched copolymer was found to be more resistant to the applied shear flow in all regimes. These findings are noteworthy because while given a certain flow strength the final count of adsorbed polymers may not differ significantly for very long simulation times, the characteristic desorption time at which polymers detach from the substrate plays a crucial role in the performance of polymer coatings for cosmetic applications.

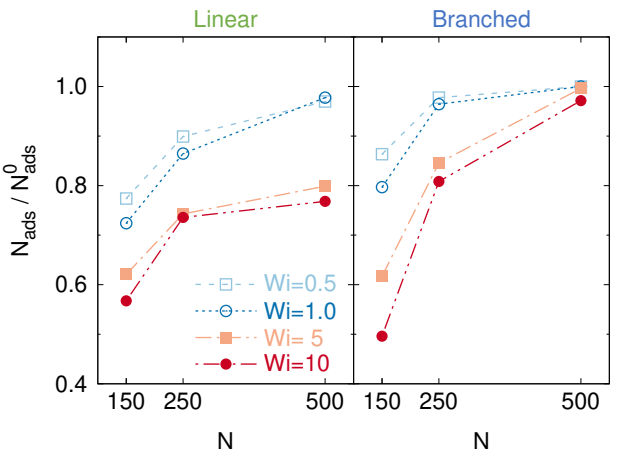

Figure 9: Fraction of adsorbed polymers on the heterogeneous substrate as a function chain length for different flow strengths, characterized by the Weissenberg number.

Further details about the final fraction of adsorbed polymers can be found in Figure 9, where the ratio between the final and initial number of adsorbed chains is plotted as a function of the degree of polymerization N for the four different flow strengths applied to the systems, characterized by the Weissenberg number. As previously mentioned, in all cases the length of the polymer chains was found to increase the stability of the polymer coatings. The final number of adsorbed chains clearly depends on the strength of the applied shear flow, although within the same regime there are not significant differences for the two values of Wi considered. While both polymer types desorb similarly under a weak shear flow, the combined effect of chain length and architecture was found to play an determinant role in the stability of the polymer coating in the strong flow regime. Except the smallest branched polymers under very strong shear flow, all the systems preserved more than 50% of the adsorbed chains. In addition, the layer formed by the largest branched polymers seemed to be unaltered for all the applied flows.

Conclusions

Developing novel sustainable formulations presents significant challenges for the industry, since replacing harmful polymers by others with natural origin is not straightforward. For cosmetic applications polysaccharides may be viable alternatives, but identifying suitable molecules requires additional research into their physical and chemical attributes. Most importantly, discerning the physical properties that influence polymer adsorption to hair-like surfaces is crucial. To investigate this issue, we generated a computational substrate mimicking a real microscopy of the external F-layer of the hair and we created models of two polymers with different architecture. We implemented coarse-grained molecular dynamics simulations with implicit solvent to observe polymer adsorption on the substrate and we executed Brownian dynamics simulations of the adsorbed polymers under a linear shear flow to evaluate the stability of the polymer coating. We characterized the polymer coating by computing concentration profiles of adsorbed polymers as a function of their distance from the substrate. Our data indicated that higher polymer concentration increased adsorption, and polymer chains showed a clear tendency to adsorb onto the substrate. Notably, the shape of the density profiles did not depend on the concentration but on the polymer type, and the branched copolymer yielded a thicker coating. To assess the uniformity of polymer coverage on the substrate, we conducted an innovative analysis, splitting the simulation box into slabs and computing two-dimensional density profiles. This analysis revealed the heterogeneous substrate pattern in the case of the linear copolymer, whereas the branched copolymer exhibited more random coverage. When assessing coating stability, we tracked the fraction of adsorbed polymers over time and found that even under weak shear flow, some chains desorbed. Under strong flow conditions, the rate and magnitude of polymer desorption increased significantly. This is a key result since desorption time can significantly impact cosmetic applications. We also noted that longer polymer chains resulted in more resistant coatings for both linear and branched polymers, although the branched layer was found to be more stable.

The findings of our study emphasize that the architecture of polymers, whether linear or branched, plays a critical role in their adsorption onto heterogeneous substrates. Interestingly, even polymers with comparable properties in bulk such as gyration radius, and similar adsorption energies with a given substrate, can display distinct behavior due to differences in architecture. This

is particularly evident when evaluating their resistance to applied shear flow. Hence the transition towards sustainable new formulations in industry is not as simple as replacing a synthetic polymer with a natural one and expecting similar results. This change requires thorough research in both polymer physics and chemistry to identify feasible polymers that can effectively replace harmful ingredients without compromising performance. Our study highlights the importance of considering not only the simple bulk properties of polymers, such as density or texture, but also their structural design, as well as the chemical complexity of the target substrate, when seeking sustainable alternatives for industrial applications.

Future studies could enhance our understanding of polymer coatings in several ways. Introducing surface roughness into the substrate model could offer a more realistic approximation of natural surfaces, providing more accurate predictions of polymer adsorption and desorption. Refinement of simulations could also involve the incorporation of additional ingredients, such as surfactants. Given their prevalence in cosmetic and industrial formulations, surfactants could substantially alter adsorption dynamics and influence the stability of polymer layers. Thus, their inclusion would provide a more detailed understanding of multi-component solutions. Furthermore, exploring the friction behavior of adsorbed polymer layers could provide insights into the sensory effects associated with different polymer coatings, a factor of critical importance in cosmetic applications.

Acknowledgement This research was supported by L'Oréal Research and Innovation. This work was performed using the the GRICAD infrastructure, supported by Grenoble research communities, and HPC resources from GENCI-IDRIS (Grant 2021-A0100912435 and 2022-AD010912435R1). I.A.B. acknowledges María Zambrano Grant funded by MCIN/AEI and NextGenerationEU/PRTR (C21.I4.P1), and the Precompetitive Research Projects Program of the University of Granada Research Plan. N.A.G. thanks PICT 2019-02257.

Conflicts of interest

G.S.L and F.L are full employees of L'Oréal involved in research activities.

Author Contributions

I.A.B. and T.I.M. performed the computations and analyzed the results. I.A.B. wrote the initial draft of the manuscript. T.I.M developed polymer models. G.C. assisted with data analysis. N.A.G. developed the numerical approach for modeling the substrate. The study was conceptualized and designed by F.L., J.-L.B., and G.S.L. All authors contributed to the interpretation of the results and the writing and revising of the manuscript.

Supporting Information Available

The Supporting Information file (PDF) includes additional information on the analysis methods used in this study. Specifically, it provides further details on the computation of the chain relaxation time, the description of the gyration tensor, and the slab analysis employed to assess the uniformity of substrate coverage.

References

(1) Anastas, P.; Eghbali, N. Green Chemistry: Principles and Practice. *Chemical Society Reviews* **2010**, *39*, 301–312, DOI: 10.1039/B918763B.

(2) Hössel,; Dieing,; Nörenberg,; Pfau,; Sander, Conditioning polymers in today's shampoo formulations – efficacy, mechanism and test methods. *International Journal of Cosmetic Science* **2000**, *22*, 1–10, DOI: https://doi.org/10.1046/j.1467-2494.2000.00003.x.

(3) Cumming, J. L.; Hawker, D. W.; Nugent, K. W.; Chapman, H. F. Ecotoxicities of polyquaterniums and their associated polyelectrolyte-surfactant aggregates (PSA) to Gambusia holbrooki. *Journal of Environmental Science and Health, Part A* **2008**, *43*, 113–117, DOI: 10.1080/10934520701781160, PMID: 18246502.

(4) Luengo, G. S.; Fameau, A.-L.; Léonforte, F.; Greaves, A. J. Surface science of cosmetic substrates, cleansing actives and formulations. *Advances in Colloid and Interface Science* **2021**, *290*, 102383, DOI: https://doi.org/10.1016/j.cis.2021.102383.

(5) Zhu, Y.; Romain, C.; Williams, C. K. Sustainable polymers from renewable resources. *Nature* **2016**, *540*, 354–362, DOI: 10.1038/nature21001.

(6) L'Haridon, J.; Martz, P.; Chenéble, J.-C.; Campion, J.-F.; Colombe, L. Ecodesign of cosmetic formulae: methodology and application. *International Journal of Cosmetic Science* **2018**, *40*, 165–177, DOI: https://doi.org/10.1111/ics.12448.

(7) Bouillon, C., Wilkinson, J., Eds. *The Science of Hair Care*, 2nd ed.; CRC Press: Boca Raton, 2005; DOI: 10.1201/b14191.

(8) Robbins, C. R. *Chemical and Physical Behavior of Human Hair*; Springer Berlin Heidelberg: Berlin, Heidelberg, 2012; DOI: 10.1007/978-3-642-25611-0.

(9) Bhushan, B. *Biophysics of Human Hair: Structural, Nanomechanical, and Nanotribological Studies*; Springer Berlin Heidelberg: Berlin, Heidelberg, 2010; DOI: 10.1007/978-3-642-15901-5.

(10) Thibaut, S. et al. Chronological ageing of human hair keratin fibres. *International Journal of Cosmetic Science* **2010**, *32*, 422–434, DOI: 10.1111/j.1468-2494.2009.00570.x.

(11) Maddar, F. M.; Perry, D.; Brooks, R.; Page, A.; Unwin, P. R. Nanoscale surface charge visualization of human hair. *Analytical chemistry* **2019**, *91*, 4632–4639.

(12) Wang, N.; Barfoot, R.; Butler, M.; Durkan, C. Effect of Surface Treatments on the Nanomechanical Properties of Human Hair. *ACS Biomaterials Science & Engineering* **2018**, *4*, 3063–3071, DOI: 10.1021/acsbiomaterials.8b00687, PMID: 33435026.

(13) Durkan, C.; Wang, N. Nanometre-scale investigations by atomic force microscopy into the effect of different treatments on the surface structure of hair. *International Journal of Cosmetic Science* **2014**, *36*, 598–605, DOI: https://doi.org/10.1111/ics.12161.

(14) Korte, M.; Akari, S.; Kühn, H.; Baghdadli, N.; Möhwald, H.; Luengo, G. S. Distribution and Localization of Hydrophobic and Ionic Chemical Groups at the Surface of Bleached Human Hair Fibers. *Langmuir* **2014**, *30*, 12124–12129, DOI: 10.1021/la500461y.

(15) Weiand, E.; Ewen, J. P.; Koenig, P. H.; Roiter, Y.; Page, S. H.; Angioletti-Uberti, S.; Dini, D. Coarse-grained molecular models of the surface of hair. *Soft Matter* **2022**, *18*, 1779–1792, DOI: 10.1039/D1SM01720A.

(16) Pastore, R.; David, A.; Casalegno, M.; Greco, F.; Raos, G. Influence of wall heterogeneity on nanoscopically confined polymers. *Phys. Chem. Chem. Phys.* **2019**, *21*, 772–779, DOI: 10.1039/C8CP06757K.

(17) Klebes, J.; Finnigan, S.; Bray, D. J.; Anderson, R. L.; Swope, W. C.; Johnston, M. A.; Conchuir, B. O. The Role of Chemical Heterogeneity in Surfactant Adsorption at Solid–Liquid Interfaces. *Journal of Chemical Theory and Computation* **2020**, *16*, 7135–7147, DOI: 10.1021/acs.jctc.0c00759, PMID: 33081471.

(18) Llamas, S.; Guzmán, E.; Ortega, F.; Baghdadli, N.; Cazeneuve, C.; Rubio, R. G.; Luengo, G. S. Adsorption of polyelectrolytes and polyelectrolytes-surfactant mixtures at surfaces: a physico-chemical approach to a cosmetic challenge. *Advances in Colloid and Interface Science* **2015**, *222*, 461–487, DOI: https://doi.org/10.1016/j.cis.2014.05.007, Reinhard Miller, Honorary Issue.

(19) Frantz, P.; Granick, S. Kinetics of polymer adsorption and desorption. *Phys. Rev. Lett.* **1991**, *66*, 899–902, DOI: 10.1103/PhysRevLett.66.899.

(20) Polotsky, A. A. Adsorption of a homopolymer chain onto a heterogeneous stripe-patterned surface studied using a directed walk model of the polymer. *Journal of Physics A: Mathematical and Theoretical* **2016**, *49*, 015001, DOI: 10.1088/1751-8113/49/1/015001.

(21) Polotsky, A. A.; Ivanova, A. S. Effect of bending stiffness on the polymer adsorption onto a heterogeneous stripe-patterned surface. *Journal of Physics A: Mathematical and Theoretical* **2022**, *55*, 375006, DOI: 10.1088/1751-8121/ac8589.

(22) Ivanova, A. S.; Polotsky, A. A. Random copolymer adsorption onto a periodic heterogeneous surface: A partially directed walk model. *Phys. Rev. E* **2022**, *106*, 034501, DOI: 10.1103/PhysRevE.106.034501.

(23) Milchev, A.; Binder, K. How does stiffness of polymer chains affect their adsorption transition? *The Journal of Chemical Physics* **2020**, *152*, DOI: 10.1063/1.5139940, 064901.

(24) Banerjee, S.; Cazeneuve, C.; Baghdadli, N.; Ringeissen, S.; Léonforte, F.; Leermakers, F. A. M.; Luengo, G. S. Modeling of Polyelectrolyte Adsorption from Micellar Solutions onto Biomimetic Substrates. *The Journal of Physical Chemistry B* **2017**, *121*, 8638–8651.

(25) Zhou, Y.; Zhang, J.; Huang, J. Dynamic Propagation Depth in Substrate-Supported Polymer Films: A Molecular Dynamics Simulation. *Macromolecules* **2023**, *56*, 2437–2446, DOI: 10.1021/acs.macromol.2c02539.

(26) Lee, J.-J.; Fuller, G. G. Adsorption and desorption of flexible polymer chains in flowing systems. *Journal of Colloid and Interface Science* **1985**, *103*, 569–577, DOI: 10.1016/0021-9797(85)90132-8.

(27) Panwar, A. S.; Kumar, S. Brownian dynamics simulations of polyelectrolyte adsorption in shear flow. *The Journal of Chemical Physics* **2005**, *122*, 154902, DOI: 10.1063/1.1876172.

(28) Ibáñez-García, G. O.; Goldstein, P.; Hanna, S. Brownian dynamics simulations of confined tethered polymers in shear flow: the effect of attractive surfaces. *The European Physical Journal E* **2013**, *36*, DOI: 10.1140/epje/i2013-13056-5.

(29) Šindelka, K.; Kowalski, A.; Cooke, M.; Mendoza, C.; Lísal, M. Interactions of cationic surfactant-fatty alcohol monolayers with natural human hair surface: Insights from dissipative particle dynamics. *Journal of Molecular Liquids* **2023**, *375*, 121385, DOI: https://doi.org/10.1016/j.molliq.2023.121385.

(30) Weiand, E.; Ewen, J. P.; Roiter, Y.; Koenig, P. H.; Page, S. H.; Rodriguez-Ropero, F.; Angioletti-Uberti, S.; Dini, D. Nanoscale friction of biomimetic hair surfaces. *Nanoscale* **2023**, *15*, 7086–7104, DOI: 10.1039/D2NR05545G.

(31) Coscia, B. J.; Shelley, J. C.; Browning, A. R.; Sanders, J. M.; Chaudret, R.; Rozot, R.; Léonforte, F.; Halls, M. D.; Luengo, G. S. Shearing friction behaviour of synthetic polymers compared to a functionalized polysaccharide on biomimetic surfaces: models for the prediction of performance of eco-designed formulations. *Phys. Chem. Chem. Phys.* **2023**, *25*, 1768–1780, DOI: 10.1039/D2CP05465E.

(32) Morozova, T. I.; García, N. A.; Barrat, J.-L.; Luengo, G. S.; Léonforte, F. Adsorption and Desorption of Polymers on Bioinspired Chemically Structured Substrates. *ACS Applied Materials & Interfaces* **2021**, *13*, 30086–30097, DOI: 10.1021/acsami.1c07425.

(33) Ma, P. L.; Lavertu, M.; Winnik, F. M.; Buschmann, M. D. New Insights into chitosan-DNA interactions using isothermal titration microcalorimetry. *Biomacromolecules* **2009**, *10*, 1490–1499.

(34) Tsereteli, L.; Grafmüller, A. An accurate coarse-grained model for chitosan polysaccharides in aqueous solution. *PLoS One* **2017**, *12*, e0180938.

(35) Grest, G. S.; Kremer, K. Molecular Dynamics Simulation for Polymers in the Presence of a Heat Bath. *Phys. Rev. A* **1986**, *33*, 3628.

(36) Brugnerotto, J.; Desbrieres, J.; Heux, L.; Mazeau, K.; Rinaudo, M. Overview on structural characterization of chitosan molecules in relation with their behavior in solution. Macromolecular Symposia. 2001; pp 1–20.

(37) Anderson, J. A.; Lorenz, C. D.; Travesset, A. General Purpose Molecular Dynamics Simulations Fully Implemented on Graphics Processing Units. *Journal of Computational Physics* **2008**, *227*, 5342–5359, DOI: 10.1016/j.jcp.2008.01.047.

(38) Brinkman, H. C. A calculation of the viscous force exerted by a flowing fluid on a dense swarm of particles. *Flow, Turbulence and Combustion* **1949**, *1*, 27–34, DOI: 10.1007/BF02120313.

(39) Milner, S. T. Hydrodynamic penetration into parabolic brushes. *Macromolecules* **1991**, *24*, 3704–3705.

(40) Dealy, J. M.; Read, D. J.; Larson, R. G. *Structure and rheology of molten polymers. From structure to flow behavior and back again*, 2nd ed.; Hanser Publishers: Munich, 2018; p 592, DOI: 10.1007/s00397-018-1118-4.